Mechanisms of prion protein assembly into amyloid

Jan Stöhr*, Nicole Weinmann*, Holger Wille[†‡], Tina Kaimann*, Luitgard Nagel-Steger*, Eva Birkmann*, Giannantonio Panza*, Stanley B. Prusiner[†‡§], Manfred Eigen[¶‖], and Detlev Riesner*[‖]

*Institut fuer Physikalische Biologie and Biologisch-Medizinisches Forschungszentrum, Heinrich-Heine-Universitaet Duesseldorf, 40225 Duesseldorf, Germany; [†]Institute for Neurodegenerative Diseases, [‡]Department of Neurology, and [§]Department of Biochemistry and Biophysics, University of California, San Francisco, CA 94143; and [¶]Max-Planck-Institut fuer biophysikalische Chemie, D-37077 Goettingen, Germany

Contributed by Manfred Eigen, December 21, 2007 (sent for review November 1, 2007)

The conversion of the α-helical, cellular isoform of the prion protein (PrP^C) to the insoluble, β-sheet-rich, infectious, disease-causing isoform (PrP^{Sc}) is the key event in prion diseases. In an earlier study, several forms of PrP were converted into a fibrillar state by using an *in vitro* conversion system consisting of low concentrations of SDS and 250 mM NaCl. Here, we characterize the structure of the fibril precursor state, that is, the soluble state under fibrillization conditions. CD spectroscopy, analytical ultracentrifugation, and chemical cross-linking indicate that the precursor state exists in a monomer-dimer equilibrium of partially denatured, α-helical PrP, with a well defined contact site of the subunits in the dimer. Using fluorescence with thioflavin T, we monitored and quantitatively described the kinetics of seeded fibril formation, including dependence of the reaction on substrate and seed concentrations. Exponential, seed-enhanced growth can be achieved in homogeneous solution, which can be enhanced by sonication. From these data, we propose a mechanistic model of fibrillization, including the presence of several intermediate structures. These studies also provide a simplified amplification system for prions.

dimer | seeding | fibril | precursor state

Prion diseases are fatal, neurodegenerative diseases that include Creutzfeldt–Jakob disease in humans, bovine spongiform encephalopathy (BSE), and scrapie in sheep. The key molecular event in prion diseases is the conformational change of a host-encoded prion protein, denoted as PrP^C, into the disease-causing isoform, PrP^{Sc} (1). Because prions do not contain any genetic information in the form of nucleic acid (2, 3), the information for prions is enciphered in the structure of the pathological isoform. Prion replication occurs by converting PrP^C to PrP^{Sc}; the pool of PrP^C is replenished by the cellular synthesis of PrP^C. Several mechanistic models have been proposed for this transfer of conformation, among them the heterodimer model (4), the cooperative model like an oligomeric enzyme (5), and the model of seeded polymerization (6). Most experimental data support the model of seeded polymerization. The transition of PrP^C into PrP^{Sc} can be induced *in vivo* either by an infection with prions, by spontaneous conversion, or by mutations in the sequence of PrP.

Regardless of the cause, the conformational change of PrP^C into PrP^{Sc} results in a fundamental change of its biophysical properties. PrP^C is membrane-bound, rich in α-helical secondary structure, soluble in mild detergents, and noninfectious, whereas PrP^{Sc} is β-sheet-rich, aggregated, and infectious (for review, see ref. 1). Proteinase K (PK) digests PrP^C completely but cleaves PrP^{Sc} specifically at residue 89 or 90 leaving the C terminus (amino acids 90–231) intact; this protease-resistant fragment is denoted PrP 27–30 and is fully infectious (7–10). If PK digestion is carried out in the presence of detergents, PrP 27–30 assembles into prion rods, which have the tinctorial properties of amyloid (11, 12).

To investigate the mechanism of prion formation, two different strategies have been pursued. In one approach, the spontaneous conversion of PrP^C or recombinant (rec) PrP in the absence of PrP^{Sc}, as in the sporadic form of prion disease, is investigated. In another approach, the PrP^{Sc}-dependent conversion of PrP, which simulates exogenous prion infection, is studied. Synthetic prions were formed from amyloidic recPrP(90–231), demonstrating that conversion of purified recPrP is sufficient for the generation of infectivity, albeit at very low titers (13, 14). Prion infectivity was also generated by protein-misfolding cyclic amplification (PMCA) in mixtures of cell extracts from brain tissue of infected and noninfected animals; by orders of magnitude, higher infectivity was obtained in the amplified samples compared with the seed used to initiate the amplification (15, 16). In a similar system, infectivity was generated also spontaneously (17).

In the present study, we examined the molecular mechanisms of spontaneous and seeded fibril formation. We identified a soluble amyloid-precursor (preamyloid) state and characterized it by analytical ultracentrifugation, chemical cross-linking, mass spectrometry, and circular dichroism. Using controlled and well defined conditions (buffers, solvents, recPrP, purified PrP^{Sc}, homogeneous incubation conditions), we quantified the kinetics of fibril formation by monitoring Thioflavin T (ThT) fluorescence. Addition of PrP^{Sc} seeds reduced the time for fibril formation from weeks to hours, and the lag phase of fibril formation depended on the recPrP concentration and on the PrP^{Sc} concentration. The sensitivity of the system could be enhanced to a detection limit of 6.5×10^{-7} brain equivalents (be) per μl of PrP^{Sc}. From these data, we propose a mechanistic model of fibril formation.

Results

***In Vitro* Formation of a Preamyloid State and Amyloid Fibers.** Previously, we described an *in vitro* conversion system, in which different conformational states of recPrP could be established by varying the concentration of SDS (18). In a follow-up study, this system was optimized to produce amyloid fibrils from recombinant and natural PrP (19). Low concentrations of SDS (0.02–0.03%), 250 mM NaCl, and a neutral buffer are essential for fibril formation. In the present study, we found that recPrP exists in the absence of PrP^{Sc} in a preamyloid state, which is stable and soluble for >7 days. In the presence of PrP^{Sc} seeds, fibrillization is substantially accelerated: Fibrils formed within 24 h.

Analysis of the Preamyloid State. recPrP in the preamyloid state was characterized by analytical ultracentrifugation, CD spectroscopy, and chemical cross-linking.

Analytical Ultracentrifugation. A sedimentation-diffusion equilibrium of recPrP under conditions of the precursor state was established in the analytical ultracentrifuge at 15,000, at 23,300, at 27,000, and at 31,600 rpm (Fig. 1*A*). The data could be fitted satisfactorily assuming a two-component system. The data revealed two different species with apparent molecular masses of 22 kDa (33.3%) and 35.2

Author contributions: J.S. and N.W. contributed equally to this work; J.S., N.W., S.B.P., M.E., and D.R. designed research; J.S., N.W., H.W., T.K., L.N.-S., E.B., and G.P. performed research; J.S., N.W., H.W., T.K., L.N.-S., E.B., M.E., and D.R. analyzed data; and J.S., N.W., S.B.P., and D.R. wrote the paper.

Conflict of interest statement: S.B.P. and D.R. have financial interest in InPro Biotechnology, Inc.

[‖]To whom correspondence may be addressed. E-mail: eigen@gwdg.de or riesner@biophys.uni-duesseldorf.de.

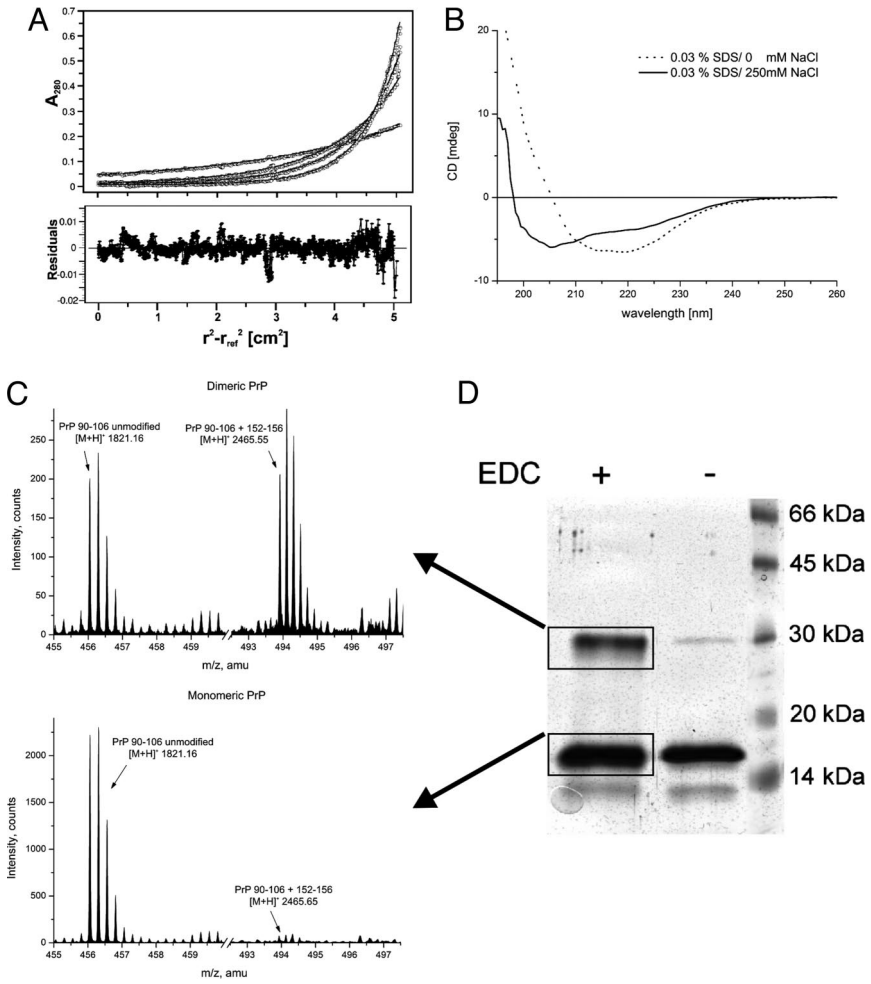

Fig. 1. Characteristics of the preamyloid state. (*A*) Sedimentation equilibrium centrifugation of recPrP after 7 days of incubation. (*Upper*) Experimental data overlaid by the fitted curves. (*Lower*) residuals. (*B*) CD spectra of recPrP in the preamyloid state in the presence (solid line) and absence of NaCl (dotted line). (*C*) LC-ESI-MS spectra of cross-linked preamyloids digested with trypsin. In the preamyloid state, cross-linking of residues 90–106 and 152–156 was not observed in monomeric recPrP (*Lower*) but was seen in dimeric recPrP (*Upper*). (*D*) Analysis of the preamyloid state after cross-linking by gel electrophoresis.

kDa (66.6%), respectively. The molecular mass of recPrP (90–231) is 16.243 kDa, which would fit into 22 kDa as a monomer with 20 molecules of SDS bound if the partial specific volume of SDS was corrected. In a similar way, the second component of 35.2 kDa can be interpreted as a dimer of recPrP with 10 molecules of SDS bound. This interpretation is in good accordance with earlier data of monomeric recPrP-SDS and dimeric recPrP-SDS complexes, although those were obtained in the absence of NaCl (18).

CD Spectroscopy. In earlier studies, the secondary structure of recPrP in 0.03% SDS but without NaCl was determined to be a soluble β-sheet-rich structure that is prone to form amorphous aggregates (18). The addition of NaCl leads to a conformation composed of α-helical and random-coil secondary structures (Fig. 1*B*). This conformation, called "α/random," polymerizes into regular fibrils (Fig. 2*A*). Naturally, a stable PrP^C-like, α-helical structure has to denature partially to form fibrils.

Chemical Cross-linking of the Contact Sites in Dimeric Preamyloid recPrP. To determine the contact sites, we cross-linked recPrP in the preamyloid state by EDC, then analyzed the sample by fully denaturing PAGE and Coomassie staining (Fig. 1*D*). This procedure was used in earlier studies to determine the molecular contact sites in an α-helical dimeric state of recPrP stabilized by 0.06% SDS in the absence of NaCl (20). A cross-linked dimeric form of recPrP was clearly detectable but in lower concentration compared with dimers in the absence of NaCl. The bands containing the recPrP monomer and dimer were cut out separately and the recPrP digested in-gel by trypsin. The samples were eluted from the gel, and the cross-linked peptides were identified by mass spectrometry according to a method described in ref. 20. In the monomeric band, no intramolecular contact sites were found, demonstrating that the N terminus in the preamyloid state is flexible. In the dimeric band, we found a contact site with cross-linked segments at residues 90–106 and 152–156 (Fig. 1*C*), which was also identified in earlier studies in the α-helical dimer (0.06% SDS, no NaCl).

Spontaneous Fibril Formation of recPrP. In the absence of PrP^{Sc} seeds, 80 ng/μl recPrP incubated with 0.03% SDS and 250 mM NaCl formed fibrils within 35 days, as described in ref. 19. Increasing the recPrP concentration to 300 ng/μl accelerated the formation of amyloid fibrils: Fibrils formed after 7 days of incubation. These fibrils were characterized by electron microscopy, ThT fluorescence, and digestion with PK. They showed the characteristic appearance of amyloid fibrils (Fig. 2*A*) and the typical increase in ThT fluorescence (Fig. 2*B*). PK digestion under harsh conditions (PrP:PK ratios of 1:20 and 1:50) revealed a protease-resistant fragment of 10–14 kDa, which remained stable even after 1 h of digestion (Fig. 2*C*). Whereas α-helical recPrP was degraded completely (Fig. 2*D*), PK digestion of mouse synthetic prions showed a roughly similar pattern of protease resistance (13, 21).

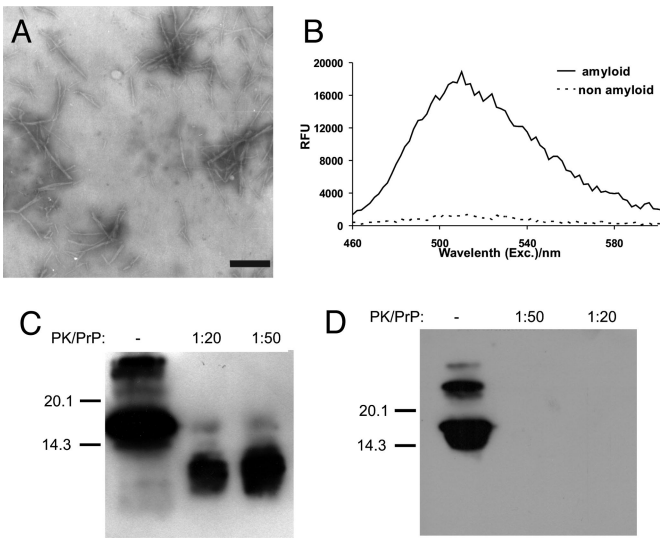

Fig. 2. Properties of recPrP amyloids. (*A*) Electron micrograph showing the typical structure of amyloid fibrils after 6 days of incubation. (Scale bar, 0.5 μm.) (*B*) Amyloid formation of recPrP (solid line) was monitored by the change in ThT fluorescence. ThT was added to a final concentration of 5 μM and a final protein concentration of 10 ng/μl. recPrP in 0.06% SDS (dotted line) is shown as a control. Protease digestion of recPrP amyloids (*C*) and α-helical recPrP (*D*) at 1:20 and 1:50 ratios (PrP:PK) demonstrate that amyloid formed from recPrP is protease-resistant. Apparent molecular masses based on the migration of protein standards are shown in kilodaltons.

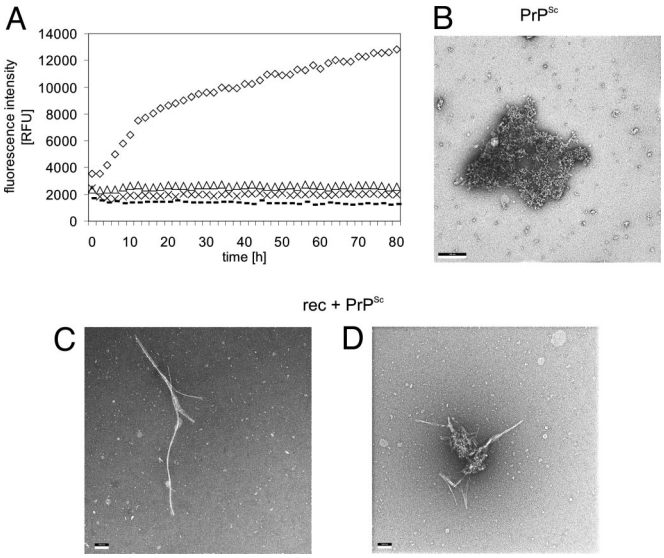

Fig. 3. Seeded fibril formation. (*A*) recPrP (80 ng/μl) seeded with purified PrP^{Sc} (diamonds) forms amyloid fibrils readily compared with controls: recPrP + uninfected 1.6×10^{-4} brain equivalents (be) per μl (×); recPrP alone (triangles); purified PrP^{Sc} alone (dashes). Fibril formation was monitored by using the ThT fluorescence assay. Electron micrograph of PrP^{Sc} aggregates after NaPTA precipitation (*B*), fibrillar recPrP (*C*), and PrP^{Sc} aggregates combined with recPrP fibrils (*D*).

PrP^{Sc}-Seeded Fibril Formation of recPrP. We analyzed the effect of PrP^{Sc} seeds on the mechanism and kinetics of fibril formation of recPrP. PrP^{Sc} seeds were prepared from the brain of an infected hamster by NaPTA precipitation (22), and negative controls were obtained in the same manner from noninfected brain tissue. To evaluate the kinetics quantitatively, we applied a homogeneous system, without the cyclic sonication of the PMCA system (15), but with thorough shaking. After resuspension in 10 mM NaPi, pH 7.2, the samples were adjusted to final concentrations of 0.025% SDS, 250 mM NaCl, and 80 ng/μl recPrP in a volume of 150–200 μl. The formation of amyloid fibrils was monitored by ThT fluorescence in 96-well plates. Seeding the reaction with purified PrP^{Sc} reproducibly accelerated the formation of amyloid fibrils of recPrP.

By using 1.6×10^{-4} be/μl of PrP^{Sc} as seeds, an increase in fluorescence intensity was observed within hours of incubation, whereas control samples showed constant, low fluorescence for the duration of the experiment (Fig. 3*A*). The kinetics can be characterized by three stages: a clear lag phase, a steep increase phase, and a slow final increase of fluorescence intensity. This seeding effect and kinetic profile were also observed in later experiments (Fig. 4*A* and *C*), in which the late phase showed saturation. Thus, fibril formation of recPrP as assayed by ThT fluorescence depends critically on the presence of PrP^{Sc} seeds.

To confirm the fibrillar character of recPrP after seeding with PrP^{Sc}, we analyzed the newly formed structures by electron microscopy (Fig. 3 *C* and *D*) and differential ultracentrifugation (data not shown). RecPrP incubated in presence of PrP^{Sc} seeds showed predominantly two structures: (*i*) a complex of newly formed fibrils grown onto the PrP^{Sc} seeds (Fig. 3*C*) and (*ii*) long fibrils, most likely detached from the PrP^{Sc} seeds (Fig. 3*D*). In comparison, the PrP^{Sc} seeds alone did not exhibit long, fibrillar structures (Fig. 3*B*), although short, fibrillar stretches might be present. Consecutive differential ultracentrifugation of recPrP after 24 h of seeded incubation resulted in a greater amount of recPrP in the pellet compared with negative controls (data not shown). Thus, these data indicate that amyloid fibrils, and not mere aggregates, were formed from the PrP^{Sc}-seeded reactions.

Concentration Dependence of PrP^{Sc}-Seeded Fibril Formation. To analyze the influence of the recPrP concentration on the seeded fibril formation, we performed the same experiment as described for Fig. 3*A*, but varied the recPrP concentration from 20 ng/μl to 160 ng/μl at a constant concentration of PrP^{Sc} seed (Fig. 4*A*). Concentrations exceeding 160 ng/μl could not be applied because spontaneous fibrillization was observed. With increasing concentrations of recPrP, the lag phase became shorter, the increase in the fluorescence signal was steeper, and the reaction saturated at a higher level. A quantitative evaluation is given in *Discussion*.

Having established that seeded formation depended on the concentration of recPrP, we examined whether the reaction depended on the concentration of the PrP^{Sc} seed as well. Determining the seed-concentration dependence enables us to quantify the fibril formation process and to establish the detection limit for PrP^{Sc}. We added varying concentrations of PrP^{Sc} seeds to 80 ng/μl of monomeric recPrP, and incubated the mixture under the same conditions as in Figs. 3*A* and 4A (Fig. 4*C*). With decreasing concentrations of PrP^{Sc} seeds, longer lag phases, slower increases in the fluorescence signals, and lower levels of saturation were observed. The lowest concentration of PrP^{Sc} seed that resulted in a clear seeding effect was 5.9×10^{-6} be/μl. At 1.9×10^{-6} be/μl and 6.5×10^{-7} be/μl, the two lowest PrP^{Sc} concentrations tested, the fluorescence signals did not increase significantly compared with controls. These data indicate the concentration dependence and the detection limit for PrP^{Sc}.

The detection limit could be further enhanced by sonication of the samples with a microtip (Bandelin sonopuls, Bandelin Electronic); samples were sonicated with 10 pulses of 0.1 s at 30% power every hour during 6 h of incubation at 37°C with continuous agitation (600 rpm) before starting measurement. Sonicated PrP^{Sc} seed at 1.9×10^{-6} be/μl resulted in an increase in the fluorescence intensity and a shortening of the lag phase (Fig. 4*C*, solid line) compared with the same concentration of PrP^{Sc} seed without sonication (Fig. 4*C*, open circle). Because our investigations focus on homogeneous incubation conditions, we chose to not pursue further the influence of sonication or other cyclic conditions.

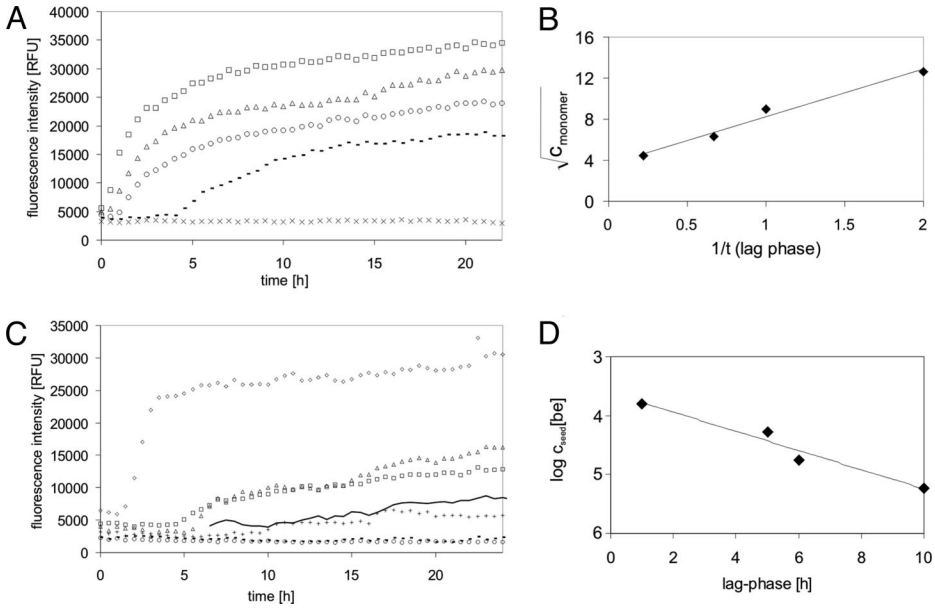

Fig. 4. Dependence of fibril formation on PrP-monomer and PrP^{Sc}-seed concentrations. Fibril formation of recPrP was monitored using ThT-fluorescence assay. (*A*) The formation of amyloid fibrils seeded with 1.6×10^{-4} be/μl PrP^{Sc} is enhanced with increasing concentrations of recPrP. The following recPrP concentrations were tested: 0 (×), 20 (dashes), 40 (circles), 80 (triangles), and 160 ng/μl (squares). (*B*) The duration of the lag phase before amyloid formation depends on $c_{monomer}$. (*C*) The formation of amyloid fibrils from 80 ng/μl of recPrP is less efficient with lower concentrations of PrP^{Sc} seed. The following concentrations of PrP^{Sc} seed were tested: 1.6×10^{-4} (diamonds), 5.3×10^{-5} (squares), 1.7×10^{-5} (triangles), 5.9×10^{-6} (pluses), 1.9×10^{-6} (circles), and 6.5×10^{-7} be/μl (dashed line). For different PrP^{Sc} concentrations, brain homogenates of infected hamsters were diluted into brain homogenates of healthy hamsters before PTA precipitation. Sonication of a sample of seeded with 1.9×10^{-6} be/μl PrP^{Sc} increased the detection limit (solid line). (*D*) The duration of the lag phase before amyloid formation depends on c_{PrPSc}.

Discussion

Since the discovery that mammalian synthetic prions could be formed from recombinantly expressed PrP(89–230) that was refolded into amyloid (13), particular attention has been drawn to the amyloid-forming pathway of PrP. We established conditions for amyloid formation [low concentration of SDS and 250 mM NaCl (19)]; recPrP in this so-called preamyloid state is soluble for at least 7 days before forming amyloid (Fig. 1).

The conditions were derived from our earlier studies of the conformational transitions of recPrP induced by varying the SDS concentration but in the absence of NaCl (19, 23). A very similar SDS-conversion system was also used successfully by other groups (24). Lowering the SDS concentration from 0.2% to 0.02%, recPrP is transformed from a monomeric, partially denatured and otherwise mainly α-helical structure through a dimer with an α-helical content similar to that of PrP^{C} and a soluble oligomeric, β-sheet-rich state to polymorphic, β-sheet-rich aggregates (25).

In a recent study (20), a structural model of the α-helical dimer was developed on the basis of chemical cross-linking data and molecular modeling. In that model, the segment 90–120, which is flexible in monomeric PrP as analyzed by NMR (26), is tightly ordered and partially involved in dimer formation. In comparison, the induction of the precursor state can be regarded as a NaCl-induced shift either from the dimeric α-helical state by simultaneously lowering the SDS concentration or from the oligomeric β-sheet-rich state at constant SDS concentration. The three structures mentioned earlier appear to be in an equilibrium, which can be shifted by both SDS and NaCl. For induction to the preamyloid state, the partially denaturing effect of NaCl on PrP appears to be essential as reported also by other groups (27). The preamyloid state is composed of monomeric and dimeric recPrP (Fig. 1*A*) and a contact site in the dimer was identified between the N-terminal amino group of Gly-90 (segment 90–106) of one PrP molecule and amino acid Glu-152 (segment 152–156) of the other. Comparison of the α-helical dimer described in ref. 20 and the preamyloid dimer revealed two important differences. First, intramolecular cross-link sites exist in the α-helical dimer but not in the precursor dimer. Second, the preamyloid dimer had a lower yield of intermolecular cross-linking. Together, these data indicate that the preamyloid state of PrP is partially denatured and otherwise α-helical, and exists as monomers and dimers.

The partial denaturation might actually be necessary for conversion of recPrP into amyloid structures; it presumably lowers the activation barrier. The preamyloid state described here and another denatured state identified previously by 0.2% SDS in the absence of NaCl (18) are likely not the same structures. In the earlier case, partial denaturation was acquired solely by SDS competing with internal hydrophobic interactions, whereas denaturation was obtained in the preamyloid state by a combination of some SDS competing with hydrophobic interactions and NaCl competing with hydrophilic interactions. Thus, the effect of NaCl cannot be attributed to the lowering of water activity and decrease in the solubility ("salting out") of the polymer, as generally known, but instead, is ascribed to a conformational change.

Our experimental findings of the preamyloid state as a partially denatured monomer and dimer fit into a model that would form the structure derived from electron crystallographic studies of PrP (28). A monomer and dimer together could form a trimer complex, which is the structural subunit of the fibrils (Fig. 5*A*). The trimer would be the steady-state intermediate for fibril formation, which is by definition not present in measurable concentrations. Individual trimers can be stacked, and the gain in free energy from stacking would drive the growth of the fibril. Also, dimers and monomers might stack on the trimeric surface. At present, we cannot decide whether two (Fig. 5*A*) or more stacked trimers are required to form the stable nucleus, so that the decay of trimers is slower than the growth of fibrils.

The aim of our studies on fibril formation of recPrP was to develop a system for seeded amplification by using purified components only (recPrP, buffer, ions, and mild denaturants). The

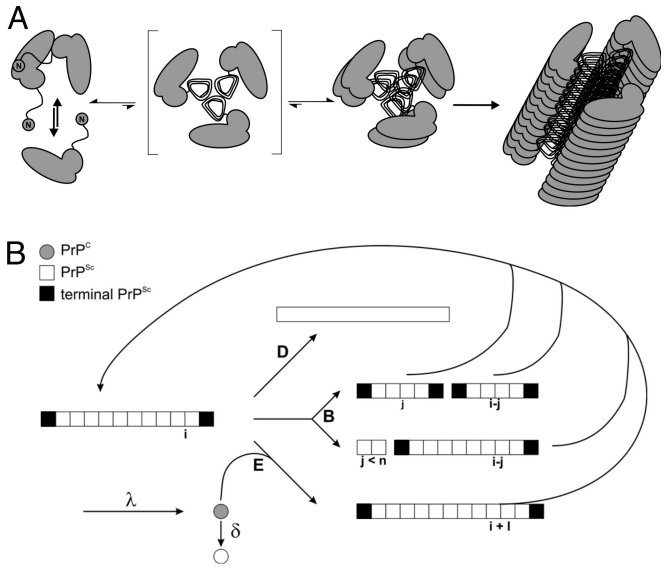

Fig. 5. Mechanistic models for PrP fibrillization. (*A*) A proposed mechanistic model depicts the preamyloid state in a monomer-dimer equilibrium, stationary state of trimer, stable nucleus of two trimers, and a growing fibril. (*B*) Reaction scheme of seeded fibrillization. For parameters, see text.

seeds, however, were naturally occurring PrP^{Sc} purified by PTA precipitation (22). Although we do not claim that no cellular factors are involved in prion infection, they are currently unknown and cannot be taken into account. Furthermore, homogeneous incubation conditions and constant rigorous shaking were applied instead of alternating incubation and sonication as in PMCA-based experiments (15, 17, 24). To differentiate amyloid formation from generalized polymorphic aggregation, we used the amyloid-specific dye ThT as a marker. Analyzing the aggregate formation by differential centrifugation, only a seed-dependent increase in aggregation was obtained, but a background of spontaneous aggregation could not be avoided. In this study, we compared spontaneous and seeded fibrillization and showed that the spontaneous process takes several weeks, whereas the seeded process approaches saturation within 1–2 days. We had to limit the concentration of recPrP to 80 ng/μl to guarantee clearly distinguishable incubation times for spontaneous and seeded fibrillization.

Masel and colleagues described prion amplification as a seed-dependent fibrillization process (29). They used a set of differential equations incorporating parameters for seed-dependent growth (Fig. 5*B*, reaction E), degradation (reaction D), and/or breakage of fibrils (reaction B), which diminishes or produces more seeds, respectively, as well as considering the synthesis (λ) and degradation of monomeric PrP (δ). We present the scheme in the form published by Eigen (30) (Fig. 5*B*); in that publication, the possibility to apply the amplification for the sensitive detection of prions was raised independently of the PMCA approach of Soto and colleagues (15). Obviously, the calculations apply to homogeneous solution conditions only, i.e., growth and breakage simultaneously.

The shape of the experimental curves of seeded fibrillization is in agreement with the scheme depicted in Fig. 5*B*. The lag phase followed by a steep increase is interpreted as an exponential growth in which both growth and generation of new seeds contribute to the curve; saturation is due to the limited monomer supply and competing reactions. The effect of breakage can be enhanced by sonication (compare curves of solid line and open circles in Fig. 4*C*). The incubation time defined by Masel and Jansen (29) as the duration required to create a well defined number of infectious particles corresponds to the *in vivo* lag phase, that is, a fixed, in our case, low level of fluorescence intensity. Because of a constant breakage rate, we can assume a constant medium size of the fibrils so that the number of particles is proportional to the fluorescence intensity. Furthermore, the concentration of monomeric PrP is assumed as constant during the lag phase. These assumptions might hold less well for very long lag phases because of degradation, denaturation, or aggregation of PrP, but these cases are not discussed here. The scheme in Fig. 5*B* and the calculations of Masel and Jansen (29) imply that the lag-phase t_l depends on concentration of seeds (c_{PrPSc}) and the concentration of monomeric PrP (c_{PrP}), respectively, as:

$$t_1 = C_1 \times \ln C_{PrPSc} + C_2 \quad \sqrt{C_{PrP}} = C_3 + \frac{C_4}{t_1}$$

C_1, C_2, C_3, and C_4 are constants that are not further evaluated here. The calculated dependence of the lag phase on substrate (C_{PrP}) and seed (C_{PrPSc}) (Fig. 4 *B* and *D*) are in agreement with the fibrillization scheme in Fig. 5*B*. Thus, our analysis confirms the three features of the scheme: exponential growth, dependence on c_{PrPSc}, and dependence on c_{PrP}. Also, the influence of sonication is in qualitative agreement; sonication breaks fibrils, thereby increases the number of seeds, and leads to a shortening of the lag phase as observed experimentally. The limited set and accuracy of the data do not allow us to evaluate parameters like growth rate, degradation rate, etc. It is not possible to extrapolate the *in vitro* lag phase to the typical incubation time in hamster that is $\approx 10^3$ times longer for the equivalent ID_{50}. If one considers, however, lower effective PrP^C levels (10×) and a clearance factor of PrP^{Sc} of 100 (31) in hamster, one would expect similarly long incubation times.

However, it is more difficult to interpret quantitatively the saturation levels. If depletion of the PrP reservoir is the only cause for plateau, then saturation levels would be proportional to c_{PrP}. Although the saturation level increases with c_{PrP}, the increase is not linear. Three types of reactions compete with fibril formation: (*i*) degradation and denaturation of PrP, (ii) degradation of fibrils and (*iii*) formation of polymorphous aggregates. As mentioned earlier, experimental evidence argues for seed-independent formation of polymorphic aggregates, which might influence the fibrillization process, particularly at later times. One might argue that competing reactions have more influence in the seeded reactions with natural PrP^{Sc}, with components from brain homogenates, compared with spontaneous fibrillization reactions.

The fibrillization system consisting only of purified, well defined components might be used as an amplification step to aid in the diagnosis of prion disease. In this homogeneous system, with sonication of the samples before measurement, we achieved a detection limit of 1.9×10^{-6} be/μl, which corresponds to titers of $\approx 10^3$-10^4 ID_{50} units, comparable to the most sensitive immunoblots (32). The method does not apply any PK digestion and can be adapted easily to prions from other species, including humans, because neither cellular brain extract from noninfected subjects nor human cell culture is needed. Despite these advantages, the homogeneous system we describe cannot attain the sensitivity of PMCA. The amplification efficiency might be further increased by using polyelectrolytes as reported by Supattapone and colleagues (17) or by using membranes as carriers for PrP and supports for the amplification.

We have to emphasize that in the present work we did not concentrate on the optimization of the diagnostic application. In a related study Prusiner and colleagues (33) described the application of a very similar technique, called amyloid seeding assay, for prion diagnosis. Under their solution conditions prions from different hosts and strains can be detected comparably well and clearly differentiated from β-amyloid seeds characteristic for Alzheimer's disease.

Our studies demonstrate a principal difficulty of employing amplification systems for disease diagnosis. Sensitivity is paramount, yet can be increased nearly indefinitely. Perhaps a prion

amplification system of intermediate sensitivity can be combined with a detection system of robust sensitivity. Alternatively, we have applied single-prion particle counting by surface-FIDA for diagnostic purposes (22, 34), which might be improved in the future by combination with an amplification system as described here.

Materials and Methods

Prion Proteins. The truncated form of recPrP of Syrian hamster residues 90–231 was used. It was expressed, purified, and refolded as described (25, 35). PrP^{Sc} was isolated to high purity by using a modified protocol of the NaPTA precipitation method (22, 36). Differing from the protocol, an additional washing step in 10 mM NaPi was performed and the resulting pellet was resuspended in 10 mM NaPi by brief sonication.

Electron microscopy, Negative Stain. A droplet of 5–10 μl containing the sample was placed on the grid and left to adsorb for 2 min. After adsorption to the grid surface, the sample was washed briefly (in 50 μl of 0.1 and 0.01 M NH_4 acetate) and stained with 2% ammonium molybdate (in 50 μl).

Circular Dichroism Spectroscopy. CD spectra were recorded with a J-715 spectropolarimeter (Jasco) in a 0.1-cm quartz cuvette at room temperature. The scanning speed was 50 nm/min with a step resolution of 1 nm. For each sample, 10 spectra were accumulated between 195 and 260 nm. The protein concentration was 100 ng/μl. Buffer spectra were subtracted from the respective protein spectra.

Analytical Ultracentrifugation. Sedimentation-diffusion equilibrium experiments were performed in a Beckman Optima XL-A analytical ultracentrifuge (Beckman Coulter) applying standard 12-mm double-sector cells at 20°C. Protein concentration distributions were recorded with a radial step size of 0.001 cm by using absorption optics at a wavelength of 230 nm or 280 nm, depending on the protein concentration. The data were analyzed by using the Global Fit procedure, which is implemented in the UltraScan II software package (Version 5.0 for UNIX) of B. Demeler (University of Texas Health Science Center, San Antonio, TX). The absorbance vs. square of the radius values was fitted to a model of two components (ideal, noninteracting) by using the Marquardt–Levenberg algorithm in the UltraScan program. Calculation of molecular mass with bound SDS per PrP was performed by using the method of Casassa and Eisenberg (37) as described in ref. 18.

Digestion with PK. recPrP (3 μg of α-helical or fibrillar) was diluted into 0.05 M Tris·HCl (pH 8.0)/100 mM NaCl/2.5 mM EDTA; then 60 ng or 150 ng of PK (for 1:20 and 1:50 PrP:PK ratios, respectively) was added. After 1 h of incubation, the reaction was stopped by addition of gel-loading buffer and heated to 95°C for 10 min.

SDS/PAGE and Western Blotting. SDS/PAGE (15%) and Western blotting were carried out according to the protocols as described in ref. 23. Anti-PrP monoclonal antibody R1 (38) was used.

Thioflavin T Assay. Fluorescence emission spectra of ThT were measured at a concentration of 5 μM ThT in 150–200 μl volumes in the absence or presence of 10 ng/μl recPrP. The spectra were recorded from 460 to 600 nm with a fixed excitation wavelength of 455 nm. Fibrillization kinetics were followed in 96-well plates as described in *Results*. For evaluation, average intensity values from 495 to 505 nm were plotted over time. All measurements were performed in a Tecan sapphire plate reader (Tecan Group).

Chemical Cross-linking of Dimers and Monomers. Dimers of recPrP were induced by diluting the protein in 0.2% SDS to fibrillization conditions (0.03% SDS and 250 mM NaCl) and incubated overnight at 25°C to achieve equilibrium conditions. The bifunctional chemical cross-linker 1-ethyl-3-(3-dimethylaminopropyl) carbodiimide hydrochloride (EDC) (Pierce) was used at a protein concentration of 6 μM and a final concentration of 1 mM EDC for 2 h (further details in ref. 20).

In-gel Digestion of Dimers and Monomers, and Analysis of the Fragments by ESI/Q-TOF Mass Spectrometry. In-gel digestion and analysis of the fragments by mass spectrometry were performed as in ref. 20.

ACKNOWLEDGMENTS. This work was supported by grants of the Bundesministerium für Bildung und Forschung, Deutsche Forschungsgemeinschaft, and the EU-Network of Excellence (NeuroPrion). T.K was a fellow of the Gruenderstiftung.

1. Prusiner SB (2007) in *Fields Virology* (Lippincott Williams & Wilkins, Philadelphia), 5th Ed, pp 3059–3091.
2. Kellings K, Meyer N, Mirenda C, Prusiner SB, Riesner D (1992) Further analysis of nucleic acids in purified scrapie prion preparations by improved return refocusing gel electrophoresis. *J Gen Virol* 73(Pt 4):1025–1029.
3. Safar JG, *et al.* (2005) Search for a prion-specific nucleic acid. *J Virol* 79:10796–10806.
4. Cohen FE, *et al.* (1994) Structural clues to prion replication. *Science* 264:530–531.
5. Eigen M (1996) Prionics or the kinetic basis of prion diseases. *Biophys Chem* 63:A1–A18.
6. Harper JD, Lansbury PT, Jr (1997) Models of amyloid seeding in Alzheimer's disease and scrapie: Mechanistic truths and physiological consequences of the time-dependent solubility of amyloid proteins. *Annu Rev Biochem* 66:385–407.
7. McKinley MP, Bolton DC, Prusiner SB (1983) A protease-resistant protein is a structural component of the scrapie prion. *Cell* 35:57–62.
8. Caughey B, Raymond GJ, Ernst D, Race RE (1991) N-terminal truncation of the scrapie-associated form of PrP by lysosomal protease(s): Implications regarding the site of conversion of PrP to the protease-resistant state. *J Virol* 65:6597–6603.
9. Pan KM, *et al.* (1993) Conversion of alpha-helices into beta-sheets features in the formation of the scrapie prion proteins. *Proc Natl Acad Sci USA* 90:10962–10966.
10. Safar J, Roller PP, Gajdusek DC, Gibbs CJ, Jr (1993) Thermal stability and conformational transitions of scrapie amyloid (prion) protein correlate with infectivity. *Protein Sci* 2:2206–2216.
11. Prusiner SB, *et al.* (1983) Scrapie prions aggregate to form amyloid-like birefringent rods. *Cell* 35:349–358.
12. McKinley MP, *et al.* (1991) Scrapie prion rod formation in vitro requires both detergent extraction and limited proteolysis. *J Virol* 65:1340–1351.
13. Legname G, *et al.* (2004) Synthetic mammalian prions. *Science* 305:673–676.
14. Legname G, et al. (2005) Strain-specified characteristics of mouse synthetic prions. *Proc Natl Acad Sci USA* 102:2168–2173.
15. Saborio GP, Permanne B, Soto C (2001) Sensitive detection of pathological prion protein by cyclic amplification of protein misfolding. *Nature* 411:810–813.
16. Castilla J, Saa P, Hetz C, Soto C (2005) In vitro generation of infectious scrapie prions. *Cell* 121:195–206.
17. Deleault NR, Harris BT, Rees JR, Supattapone S (2007) From the Cover: Formation of native prions from minimal components in vitro. *Proc Natl Acad Sci USA* 104:9741–9746.
18. Leffers KW, *et al.* (2004) The structural transition of the prion protein into its pathogenic conformation is induced by unmasking hydrophobic sites. *J Mol Biol* 344:839–853.
19. Leffers KW, *et al.* (2005) Assembly of natural and recombinant prion protein into fibrils. *Biol Chem* 386:569–580.
20. Kaimann T, *et al.* (2007) Molecular model of an α-helical prion protein dimer and its monomeric subunits as derived from chemical cross-linking and molecular modeling calculations. *J Mol Biol*, 10.1016/j.jmb2007.11.035.
21. Bocharova OV, Breydo L, Salnikov VV, Gill AC, Baskakov IV (2005) Synthetic prions generated in vitro are similar to a newly identified subpopulation of PrPSc from sporadic Creutzfeldt-Jakob Disease. *Protein Sci* 14:1222–1232.
22. Birkmann E, *et al.* (2006) Detection of prion particles in samples of BSE, scrapie by fluorescence correlation spectroscopy without proteinase K digestion. *Biol Chem* 387:95–102.
23. Post K, *et al.* (1998) Rapid acquisition of beta-sheet structure in the prion protein prior to multimer formation. *Biol Chem* 379:1307–1317.
24. Atarashi R, *et al.* (2007) Ultrasensitive detection of scrapie prion protein using seeded conversion of recombinant prion protein. *Nat Methods* 4:645–650.
25. Jansen K, *et al.* (2001) Structural intermediates in the putative pathway from the cellular prion protein to the pathogenic form. *Biol Chem* 382:683–691.
26. Liu H, *et al.* (1999) Solution structure of Syrian hamster prion protein rPrP(90–231). *Biochemistry* 38:5362–5377.
27. Apetri AC, Surewicz WK (2003) Atypical effect of salts on the thermodynamic stability of human prion protein. *J Biol Chem* 278:22187–22192.
28. Govaerts C, Wille H, Prusiner SB, Cohen FE (2004) Evidence for assembly of prions with left-handed beta-helices into trimers. *Proc Natl Acad Sci USA* 101:8342–8347.
29. Masel J, Jansen VA (2004) Prion kinetics. *Biophys J* 87:728.
30. Eigen M (2001) BSE und das Prionen-Problem. *Spek Wiss* 4:40–49.
31. Safar JG, *et al.* (2005) Prion clearance in bigenic mice. *J Gen Virol* 86:2913–2923.
32. Thomzig A, Kratzel C, Lenz G, Kruger D, Beekes M (2003) Widespread PrPSc accumulation in muscles of hamsters orally infected with scrapie. *EMBO Rep* 4:530–533.
33. Colby DW, Zhang J, Wang S, Groth D, Legname G, Riesner D, Prusiner SB (2007) Prion detection by an amyloid seeding assay. *Proc Natl Acad Sci USA* 104:20914–20919.
34. Birkmann E, *et al.* (2007) Counting of single prion particles bound to a capture-antibody surface (surface-FIDA). *Vet Microbiol* 123:294–304.
35. Mehlhorn I, *et al.* (1996) High-level expression and characterization of a purified 142-residue polypeptide of the prion protein. *Biochemistry* 35:5528–5537.
36. Safar J, *et al.* (1998) Eight prion strains have PrP(Sc) molecules with different conformations. *Nat Med* 4:1157–1165.
37. Casassa EF, Eisenberg H (1964) Thermodynamic analysis of multicomponent solutions. *Adv Protein Chem* 19:287–395.
38. Williamson RA, *et al.* (1998) Mapping the prion protein using recombinant antibodies. *J Virol* 72:9413–9418.